Applied Geochemistry 97 (2018) 93–101

Contents lists available at ScienceDirect

Applied Geochemistry

journal homepage: www.elsevier.com/locate/apgeochem

Investigation of partial water saturation effects on diffusion in shale

Jacob A. Nunn[a,*], Yan Xiang[b], Tom A. Al[a,**]

[a] Department of Earth and Environmental Science, University of Ottawa, 25 Templeton St., Ottawa, ON, K1N 6N5, Canada
[b] Department of Earth Sciences, University of New Brunswick, Fredericton, NB, Canada

ARTICLE INFO

Keywords:
Diffusion
X-ray radiography
Nuclear waste management
Partial saturation
Gas saturation
Sedimentary rock
Archie's law
Shale
Low-permeability

ABSTRACT

A new method for testing the effect of partially saturated conditions on aqueous diffusion was developed using samples from the Upper Ordovician Queenston Formation shale from the Michigan Basin of southwest Ontario, Canada. Effective diffusion coefficients (D_e) were determined for iodide tracer on duplicate cm-scale samples from a core segment. Partially saturated conditions were created with a new gas-ingrowth method that takes advantage of the variability of N_2 solubility with pressure. The method is designed to create partially saturated pores, quantify the level of partial gas/brine saturation within the tracer-accessible pore space, and measure D_e under fully porewater-saturated and partially gas-saturated conditions for the same sample. X-ray radiography is used with an iodide tracer for quantifying the degree of partial saturation and measuring D_e. The saturated D_e values range from 2.8×10^{-12} to 3.1×10^{-12} m^2/s. Following generation of a gas phase in the pores (average gas saturations of 4–6.7%), D_e values decrease by 20–22% relative to the porewater-saturated condition, indicating that the tortuosity factor (ratio of constrictivity to tortuosity) is sensitive to saturation. The data suggest that a relatively small fraction of the pore space dominates the solute transport. The gas-ingrowth method was successful for generating partial gas saturation, but the distribution of the gas phase is non-uniform, with relatively high gas saturations near boundaries and lower saturations in the interior of the samples.

1. Introduction

Low-permeability sedimentary rocks are of scientific interest because they present barriers to the migration of fluids and contaminants, which is important in CO_2 sequestration, shale gas exploitation, and nuclear waste management (Al et al., 2015; Benson and Cole, 2008; Javadpour et al., 2007; Leung et al., 2014; Lindeberg and Bergmo, 2003; Mazurek et al., 2011; Russell and Gale, 1982). Diffusion is the dominant transport process in sedimentary formations when hydraulic conductivity (K) is less than about 10^{-10} m/s. The role of diffusive transport and its effect on barrier performance requires reliable measurements of effective diffusion coefficients (D_e) (Shackelford, 1991). Measurements of D_e have been conducted at the laboratory scale (cm) with several established techniques, including: through diffusion (Jacops et al., 2013; Rebour et al., 1997; Savoye et al., 2010; Van Loon et al., 2003a, 2003b; Xiang et al., 2016), in-diffusion (Cormenzana et al., 2003), out-diffusion (Waber and Smellie, 2008), radial diffusion (Van der Kamp et al., 1996; Van Loon et al., 2004), X-ray computed tomography (Agbogun et al., 2013a; b), and radiography (Cavé et al., 2009; Loomer et al., 2013; Tidwell et al., 2000; Xiang et al., 2013). Drilling and sample collection for laboratory-scale measurements may cause thermo-mechanical disruption of cores, resulting in altered physical properties such as porosity and tortuosity. Attempts have been made to reproduce in-situ temperature and pressure conditions in the laboratory in order to determine the magnitude of these effects on diffusive transport (Savoye et al., 2011; Van Loon et al., 2003a, 2004, 2003b; Wise and Houghton., 1966; Xiang et al., 2016). In efforts to understand diffusive transport at a larger scale (10's to 100's of m), numerous researchers have employed measurements of naturally-occurring tracer distributions in rock porewater which, combined with solute-transport modelling and knowledge of paleohydrology, allows for estimation of D_e at the formation scale (Al et al., 2015; Bensenouci et al., 2011; Desaulniers et al., 1981; Gimmi et al., 2007; Hendry et al., 2004, 2013; Hendry and Harrington, 2014; Mazurek et al., 2011; Patriarche et al., 2004a, 2004b; Remenda et al., 1994).

The majority of laboratory-scale investigations have been conducted on fully saturated samples, but under in-situ conditions, partial saturation is expected in some circumstances. Examples include organic-rich sedimentary rocks that contain $CH_{4(g)}$ at concentrations in excess of solubility, resulting in exsolution and displacement of porewater, as well as tunnelling excavations, which can lead to partially saturated conditions in the Excavation Damaged Zone (EDZ) (Matray et al., 2007;

* Corresponding author.
** Corresponding author.
E-mail addresses: jnunn061@uottawa.ca (J.A. Nunn), tom.al@uottawa.ca (T.A. Al).

https://doi.org/10.1016/j.apgeochem.2018.08.004
Received 27 February 2018; Received in revised form 9 July 2018; Accepted 3 August 2018
Available online 09 August 2018
0883-2927/

Nagra, 2008). Investigations by Savoye et al. (2010, 2012, 2014, 2017) provide the most comprehensive assessment of the effect of partial saturation on solute diffusion in clay-rich rocks. They measured D_e for various tracers in the Callovo-Oxfordian claystone under partially saturated conditions using the through diffusion method and demonstrated that partial gas saturation leads to a decrease in D_e for solutes in the aqueous phase. For iodide, the tracer which is used for the present study, they observed a decrease in the effective diffusion coefficient of Iodide (D_{e-I}) by a factor of 50 under conditions of 19% gas saturation. Additional examples of diffusion studies on partially saturated geologic materials include Badv and Faridfard (2005) Conca and Wright (1992), Hamamoto et al. (2009), Hamamoto et al. (2010), Mehta et al. (1995), Olesen et al. (2000), Porter et al. (1960) and Rowell et al. (1967).

The Upper Ordovician shales (Queenston, Georgian Bay and Blue Mountain formations) of the Michigan Basin in southwest Ontario, Canada, have been studied extensively at the Bruce nuclear site, where the 200-m thick, low-permeability shale sequence has the necessary properties to act as natural geologic barrier for a proposed Deep Geological Repository (DGR) for low- and intermediate-level radioactive waste (CEAA, 2015).

Elevated $CH_{4(g)}$ concentrations have been measured in these shales (Clark et al., 2013), and it has been suggested that a gas phase of up to 10% may be present (Intera, 2011). The porewater in the shales has very high salinity, up to halite saturation (Al et al., 2015), and dewatering methods, such as that employed by Savoye et al. (2010, 2012, 2014, 2017), would lead to salt precipitation that could occlude pores and influence D_e. The objectives of this work were to 1) develop a novel gas-ingrowth method for generation of a gas phase by manipulating pressure to control $N_{2(g)}$ solubility; and 2) measure the degree of gas saturation in the pore space using a non-destructive X-ray radiography technique (Cavé et al., 2009); 3) quantify the change in D_e for I^- that results from the generation of partial gas saturation in samples of shale from the Michigan Basin.

2. Material and methods

2.1. Sample description

The samples used in this study are from the Ordovician Queenston Formation shale. The duplicate samples were collected from a 76-mm-diameter drill core segment at a depth of 472 m in borehole DGR-3 located at the Bruce nuclear site in southwest Ontario, Canada. Representative physical and mineralogical properties of the Queenston shale are provided in Table 1.

2.2. Measurement of diffusion coefficients and porosity

2.2.1. Sample preparation and apparatus

Samples for diffusion measurements were prepared in duplicate using a diamond coring bit to drill sample cores from the original 76-mm core sample. The samples (20-mm diameter and 20–23 mm length) were drilled normal to bedding, using air to cool the bit. Natural porewater in the Queenston shale is near saturation with respect to halite (Al et al., 2015; Clark et al., 2013) so any evaporation during sample preparation could result in halite precipitation and occlusion of the pores. In order to prevent this from affecting the porosity and diffusion measurements, a new approach was used whereby samples were initially resaturated in a closed chamber containing an open vessel with deionized water. The water chemical potential gradient between the deionized water and the sample porewater causes water transfer to the rock porewater via the vapor phase. Resaturation is accomplished by vapor-phase diffusion, and at the point when water droplets began to accumulate on the surface of the rock, the samples were fully immersed in a synthetic pore water (SPW; Table 2) formulated for the Queenston shale using methods modified after the approach of Cavé et al. (2009) and Xiang et al. (2013). The samples were immersed in SPW under vacuum for four weeks prior to the start of experiments. Water-accessible porosity (ϕ_w) measurements were conducted on the rock material remaining after subcoring using the method described by Xiang et al. (2013). It is a gravimetric method that accounts for the porewater salinity and requires oven drying at 105 °C.

A diffusion cell (Fig. 1) was specially designed to prevent expansion of the sample under the increased pressures experienced during nucleation and expansion of a gas phase in the pores (see below). An initial confining pressure of 0.83 MPa was applied to the samples using a calibrated relationship between vertical load and torque on the threaded end caps of the diffusion cell, similar to the approach employed by Van Loon et al. (2003a, 2003b). This confining pressure was intended to prevent expansion and damage to the sample during nucleation and growth of a gas phase, and it has no relationship to the confining pressure that affects the Queenston shale in natural subsurface conditions (12 MPa, Xiang et al., 2016). The cell was constructed with Delrin®, a form of polyoxymethylene thermoplastic, which was

Table 1
Representative physical properties of the Queenston Formation shale, including porosity, diffusivity, hydraulic conductivity and mineralogy.

Porosity, Diffusion and Hydraulic Conductivity				
Water-accessible porosity ϕ_w[a]	Iodide-accessible porosity ϕ_I[a]	Effective-diffusion of HTO (perpendicular to bedding) $D_{e\text{-}HTO}$[a] m^2/s	Effective-Diffusion of Iodide (perpendicular to bedding) $D_{e\text{-}I}$[a] m^2/s	Hydraulic Conductivity K_h[b] m/s
0.058–0.11	0.044–0.094	4.8×10^{-12}	1.20×10^{-12} – 3.4×10^{-12}	3.0×10^{-14}

Mineralogy (wt %)			
	DGR2[c]	DGR3[d]	DGR4[d]
Quartz	4.0–12.0	23.5–34.1	18.5
K-feldspar	< 2	1.4–3.2	1.3
Plagioclase	< 2	1.2–1.9	1.9
Calcite	8.0–57.0	6.1–14.6	31.6
Dolomite/ankerite	7.0–31.0	6.6–11.4	7.6
Clay minerals	29.0–53.0	41–45.2	36.6
Illite/mica[e]	–	58.2–60.9	60.1
Illite/smectite[e]	20–39	9.7	11.9
Chlorite[e]	9.0–14.0	29.1–39.1	24.5
Kaolinite[e]	< 1	3	3.5
Pyrite	–	2.2	0.5
Hematite	–	0.12	2.1
Organic C	< 0.1–0.3	–	0.13

[a] Xiang et al. (2013).
[b] Beauheim et al. (2014).
[c] Koroleva et al. (2009).
[d] Jackson (2009).
[e] Values are expressed as wt% of the clay fraction.

Table 2
Composition of SPW and iodide tracer solution (SPW-T) used in diffusion experiments.

	SPW	SPW-T
Density (kg/L)	1.22	1.32
Element	mol/kgw	mol/kgw
Na	2.61	2.61
K	0.11	0.11
Ca	1.91	1.91
Mg	0.27	0.27
Cl	7.05	6.05
Br	0.06	0.06
Sr	0.02	0.02
I	0.00	1.00

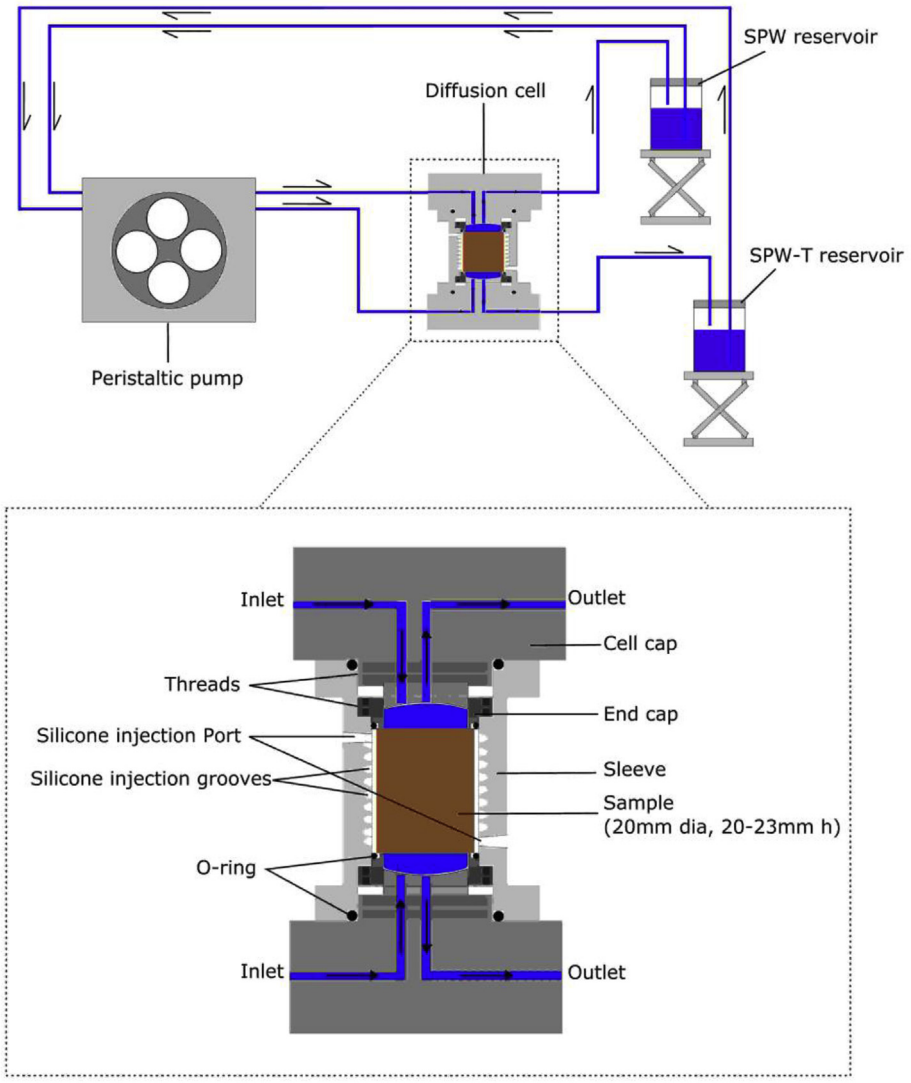

Fig. 1. Schematic diagram of the diffusion cell and experimental setup.

chosen for its rigidity and low X-ray attenuation and scattering properties. The silicone injection groves are created in a continuous spiral around the inner surface of the sleeve, allowing silicone to be injected in one of the ports and fill the annular space between the sample and the sleeve, forming an effective seal (Fig. 1).

2.2.2. Experimental procedures

Four sequential experimental procedures were performed on each of the duplicate samples (Fig. 2); first, samples were fully saturated with SPW, then in-diffusion experiments were conducted to establish diffusion coefficients for fully brine-saturated samples, the samples were then subjected to the gas generation procedure followed by measurement of the gas-saturation profiles, and finally, out-diffusion experiments were conducted to measure diffusion coefficients with the gas phase present.

Diffusion measurements were conducted using the X-ray radiography technique described by Cavé et al. (2009) based on X-ray absorption by an aqueous iodide tracer (I^-). The method can be used to spatially resolve tracer concentrations through time, allowing for determination of pore diffusion coefficients (D_p), and measurement of I^- accessible porosity (ϕ_I). Values of ϕ_I were determined for brine-saturated samples and for partially desaturated samples ($\phi_{I\text{-}g}$). A least squares regression analysis was used to obtain values for D_p by optimizing the fit between experimental data and the analytical solution to Fick's law (Crank, 1979):

$$C_i(x, t) = C_0 erfc\frac{x}{\sqrt[2]{D_p t}} \quad [1]$$

Were C_i is the concentration of tracer at distance x from the diffusion boundary at time (t) since the start of diffusion; C_0 is the concentration of tracer at the influx boundary, L is the maximum diffusion path length, equal to the sample thickness, and *erfc* is the complimentary error function. The following initial and bounding conditions apply (Crank, 1979; Shackelford, 1991):

$$C_{(x,t)} = 0 \left| \begin{matrix} t = 0 \\ x > 0 \end{matrix} \right.$$

$$C_{(x,t)} = C_0 \left| \begin{matrix} t \geq 0 \\ x = 0 \end{matrix} \right.$$

$$C_{(x,t)} = 0 \left| \begin{matrix} t \geq 0 \\ x = L \end{matrix} \right.$$

Measurements were conducted with an X-ray CT system (Pinnacle X-ray Systems, Atlanta, Georgia) equipped with a Varian® NDI-160/22 source coupled to a Gulmay® CPL series (CP2-1402) 3000 W generator and a Varian PaxScan®1313DX amorphous-silicon flat-panel imaging detector. All data were collected as 16-bit tiff image files. Acquisition

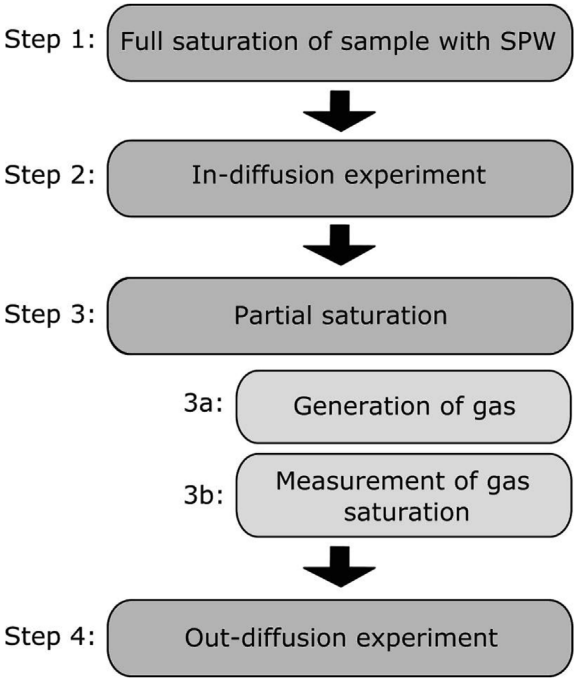

Fig. 2. Experimental procedures undertaken for a given sample.

parameters were; 1 s exposure per frame, 32 frame averages per image, source voltage of 50 kV with 60 mA current, and source filtration with 3.3 mm aluminum. Prior to the start of diffusion experiments, the fluid reservoirs at the top and bottom of the diffusion cell (Fig. 1) were filled with SPW solution. Experiments were initiated by replacing SPW in the lower reservoir with I^- tracer solution prepared from the SPW by substituting NaCl with NaI (Table 2). Reference images (radiographs) were collected immediately after tracer solution was injected and images were collected twice a day for the first two days, once a day for the following three days, and then the time interval increased to once every three-four days. All radiographs were collected with identical sample positioning and instrumental operating conditions. In all cases, pixel grey scale values from the radiograph images were converted to one-dimensional profiles that represent X-ray attenuation coefficients (μ) according to the method described by Cavé et al. (2009).

Diffusion was monitored in this way until tracer breakthrough occurred at the top boundary. The samples were then saturated with the I^- tracer solution by allowing in-diffusion from both ends. The influx of tracer was monitored by X-ray radiography over a period of eight to nine weeks until no further change in X-ray attenuation was observed. At this point, one-dimensional profiles of ϕ_I and C/C_0 were obtained following the method described by Cavé et al. (2009) and Agbogun et al. (2013a, 2013b). Relative concentration profiles allow for determinations of D_p by fitting experimental data to Equation (1), and when profiles are collected at different times the resulting D_p values can be averaged to find a representative value for the sample and the standard deviation provides an estimation of the variability associated with D_p. Repeat measurements were conducted on several samples to assess uncertainty in the C/C_0 profiles due to instrumental positioning and source/detector variability. The point-to-point uncertainty, expressed as a relative standard deviation (RSD), is 0.39% which translates to an uncertainty in iodide concentration of 0.004 mol/kgw.

2.3. Partial gas saturation

The fully tracer-saturated samples were subjected to partial gas generation with an approach that uses N_2 gas and takes advantage of the variability of N_2 solubility versus pressure as indicated by Henry's law (Equation (2)):

$$S_i = K_{H_i} P_i \quad [2]$$

where S_i is the solubility of gas i (mol/L) in an aqueous solution; K_H is the Henry's constant ($mol \cdot L^{-1} \cdot atm^{-1}$ or M/atm); P_i is the partial pressure (atm). However, with increasing gas pressures the solubility-pressure relationship becomes non-linear and deviates from Henry's law. The solubility of N_2 in high ionic strength aqueous solutions (up to 7.7 mol/L) at 25 °C can be calculated as a function of partial pressure, P_{N2}, using the model reported by Mao and Duan (2006). Calculations for the Queenston shale were conducted at the 7.7 mol/L ionic-strength limit of the model although the SPW was a Na-Ca-Cl solution with ionic strength of 9.2 mol/kgw. As a result, the N_2 solubility in SPW will be slightly overestimated by the model.

The method for generating partial saturation is based on the premise that changes in N_2 partial pressure from high (P_1) to low (P_2) causes the solubility of N_2 to decrease with the result that gas bubbles will form in the solution. For a brine solution occupying the pore spaces in a rock sample, gas bubbles should form in the pore spaces. If equilibrium is established at P_2, using the Henry's law approach, the moles of N_2 bubbles (n) can be calculated according to:

$$n_{bubble} = K_H V_p (P_1 - P_2) \quad [3]$$

where, V_p is the volume of the rock pores (L) initially occupied by brine. The volume of the gas bubbles (V_{bubble}; L) formed at P_2 can be calculated using the ideal gas law:

$$V_{bubble} = \frac{K_H V_p (P_1 - P_2) RT}{P_2} \quad [4]$$

If we assume that Henry's law and the ideal gas law are valid, the predicted volume occupied by gas (S_g) will be:

$$S_g = \left[\frac{K_H (P_1 - P_2) RT}{P_2} \right] * 100\% \quad [5]$$

As noted previously, Henry's law does not accurately represent the gas solubility at high ionic strengths and, more importantly, it is not expected that the ideal gas law, as presented in Equation (5), can accurately represent gas bubble formation in the confined pore space of clay-rich rocks. In order for gas bubbles to nucleate and grow, porewater must be expelled from the system, so the process is limited by the relative permeability for the aqueous phase, which decreases with time due to the formation of the gas phase. Also, during the time required to expel porewater, N_2 will be lost from the system by diffusion in both the aqueous phase and, increasingly, in the growing gas phase. For these reasons, it is expected that the volume of gas phase created in the pore spaces will be lower than that predicted by Equation (5). X-ray radiography was used to quantify the final degree of N_2 saturation, but the method is limited to measurements of gas saturation in the tracer-accessible pore space.

As a first step toward inducing partial gas saturation, the diffusion cells, with end caps removed, were immersed for 33 days in I^- tracer solution inside a pressure vessel with 68 atm $N_{2(g)}$ in the head space. The high N_2 gas pressure causes an increase in N_2 solubility, allowing for diffusion of elevated aqueous N_2 concentrations throughout the pore space of the rock. Based on the D_p values determined for I^- by in-diffusion, the time period of 33 days was considered sufficient to achieve 90–100% of the fully-equilibrated N_2 distribution in the sample. In the second step, the $N_{2(g)}$ overpressure in the head space was decreased to 1 atm which initiates nucleation and growth of $N_{2(g)}$ bubbles in the pore spaces, forcing tracer solution out of the sample. The evolution of partial gas saturation was monitored by X-ray radiography, and five days were sufficient for equilibration of the gas and brine saturation states. After equilibration between the gas phase and the tracer-containing brine, one-dimensional profiles of μ were collected again and used to obtain 1-D profiles of the I^-- accessible

porosity in the presence of the gas phase ($\phi_{I\text{-}g}$). The ratio between $\phi_{I\text{-}g}$ and ϕ_I was used to determine the fraction of gas saturation ($S_{g\text{-}I}$) in the I^- accessible pore fraction.

$$S_{g-I} = \left[1 - \left(\frac{\phi_{I-g}}{\phi_I}\right)\right]100\% \quad [6]$$

Anion exclusion in clay-rich rocks leads to a condition where $\phi_I < \phi_w$, so it's important to note that these reported values for $S_{g\text{-}I}$ represent fractions of ϕ_I, rather than ϕ_w. In order to represent the gas-saturation values as a fraction of ϕ_w, we multiply by the fraction of anion-accessible porosity (f_a):

$$S_{g-w} = f_a \cdot S_{g-I} \quad where: \; f_a = \phi_I/\phi_W \quad [7]$$

The use of this relationship assumes that gas-bubble nucleation and growth occurs in the largest connected pores, which are also the anion-accessible pores. This assumption is consistent with known relationships between capillary-pressure and saturation.

Out-diffusion experiments were initiated with the partially-saturated samples by introducing SPW (no tracer) into the reservoir that previously contained tracer for the in-diffusion experiments. In order to eliminate density effects, the cell was upended to maintain the higher-density solution (Table 2) at the bottom boundary. Radiographs were collected at different times using the same time increments as for the in-diffusion experiments.

3. Results and discussion

3.1. Porosity

Measurements of ϕ_w range from 0.101 to 0.103 (Table 3) and provide representative values at the sample scale, but they give no indication of smaller scale variability. Alternatively, X-ray radiography provides 1-D spatially-resolved measurements of ϕ_I (Cavé et al., 2009; Tidwell et al., 2000). These measurements indicate that there are mm-scale cyclical changes in porosity across the samples in the direction normal to bedding (Fig. 3). These features were initially thought to be due to bedding and grain-size controlled porosity variations, but petrographic examination by scanning electron microscopy (SEM) revealed that they reflect bedding-parallel dolomite-cemented lenses; the dolomite domains having lower porosity than the surrounding aluminosilicate (shale) domains (Fig. 4). There is a larger-scale variation in porosity evident in both samples, with the highest porosity (approximately 0.065–0.070) at the influx boundary, reaching a minima of approximately 0.051-0.055 at a distance of 0.014 m, and then increasing slightly with increasing distance (Fig. 3). Average ϕ_I values derived from the 1-D profiles for brine-saturated samples range between 0.054 and 0.059 and their standard deviations reflect the internal variability in each sample (Table 3). These measurements indicate that the fraction of anion-accessible porosity (f_a), represented by ϕ_I/ϕ_w ranges from 0.53 to 0.58 (Table 3). This is consistent with data reported by Xiang et al. (2013) and with previous research that

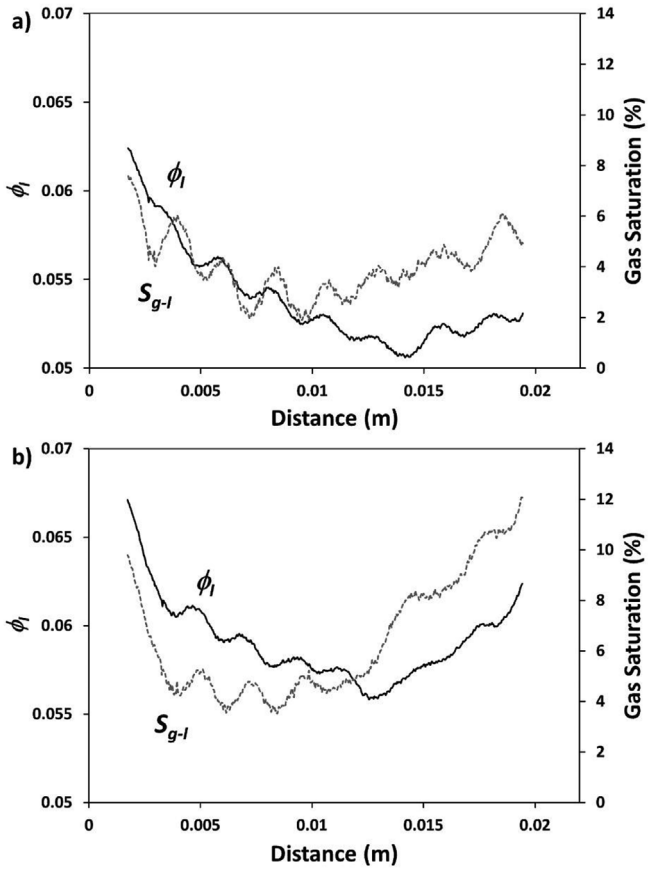

Fig. 3. Profiles for the spatial distribution of ϕ_I and gas saturation ($S_{g\text{-}I}$ %) in samples a) DGR3-472-A, and b) DGR3-472-B. Note that $S_{g\text{-}I}$ % values are relative to the total iodide-accessible porosity. The combined geometry of the samples and the cone-shaped X-ray beam causes some minor blurring of the signal near the boundaries, resulting in loss of data over a small distance.

indicates anion-accessible porosity in clay-rich rocks is lower than the total water-accessible porosity (Appelo et al., 2010; Bazer-Bachi et al., 2006; Descostes et al., 2008; García-Gutiérrez et al., 2006; Mazurek et al., 2015; Van Loon et al., 2003a, 2003b, 2007).

3.2. Diffusion in saturated shale

Profiles of relative tracer concentrations (C/C_0) collected at different times in the porewater-saturated samples are shown in Fig. 5a and b. The $D_{p\text{-}I}$ values derived from fitting the experimental data to the analytical model (Equation (1)) range from 4.8×10^{-11} to 5.8×10^{-11} m^2/s (Table 3). These values can be transformed to the more commonly reported effective diffusion coefficient (D_e):

Table 3
Comparison of results from in-diffusion measurements on fully saturated samples to out-diffusion measurements on partially saturated (PS) samples.

Sample	DGR3 472.56-A	DGR3 472.56-A-PS	DGR3 472.56-B	DGR3 472.56-B-PS
Water accessible porosity (ϕ_w)	0.101–0.103			
Iodide accessible porosity (ϕ_I)	0.054 ± [0.0030]	0.052 ± [0.0026]	0.059 ± [0.0024]	0.055 ± [0.0024]
f_a [a]	0.53		0.58	
$S_{g\text{-}I}$ % [b]	0	4.0 ± [1.1]	0	6.7 ± [2.6]
D_p (m^2/s)	$5.8 \times 10^{-11} \pm 2.6 \times 10^{-12}$	$4.8 \times 10^{-11} \pm 1.5 \times 10^{-12}$	$4.8 \times 10^{-11} \pm 2.9 \times 10^{-12}$	$4.2 \times 10^{-11} \pm 3.1 \times 10^{-12}$
ΔD_p (%)	18.9		13.3	
D_e (m^2/s)	$3.1 \times 10^{-12} \pm [2.4 \times 10^{-13}]$	$2.5 \times 10^{-12} \pm [1.5 \times 10^{-13}]$	$2.8 \times 10^{-12} \pm [2.3 \times 10^{-13}]$	$2.3 \times 10^{-12} \pm [2.2 \times 10^{-13}]$
ΔD_e (%)	22.3		20.3	

[a] Values of f_a are calculated from ϕ_I and ϕ_w measurements on adjacent samples.
[b] Gas saturation values are relative to ϕ_I.

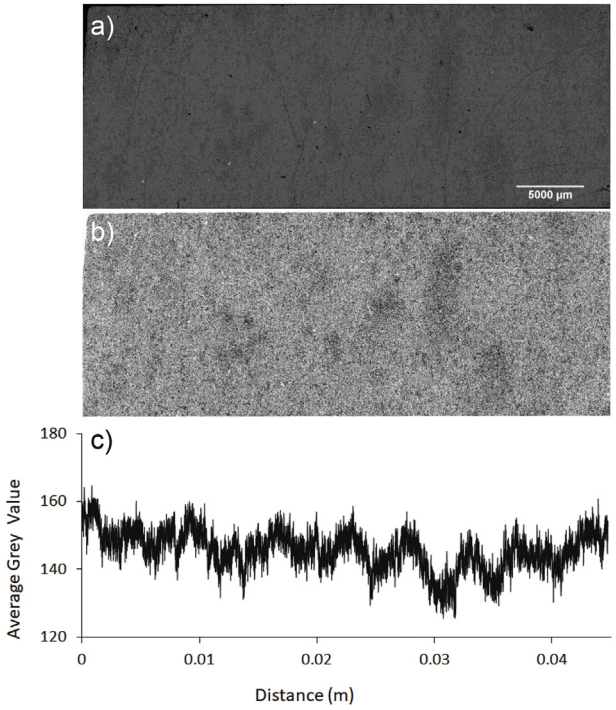

Fig. 4. a) A back-scattered-electron image from a petrographic thin section prepared directly adjacent to the diffusion samples. The plane of the section is oriented normal to bedding. b) A binary image of the region shown in a), binarized using grey-scale thresholding to emphasize dolomite-rich regions (black). c) A profile generated from the binary image and displaying the average grey value for each column of pixels versus distance. The cyclical variability represents dolomite-cemented regions that have relatively low porosity.

$$D_e = D_p\phi_I = \frac{\delta}{\tau^2}D_0\phi_I \quad [8]$$

where δ is the pore constrictivity, τ is the tortuosity and D_0 is the free-water diffusion coefficient. The constrictivity and the tortuosity cannot be measured independently and are often combined in one tortuosity factor τ_f:

$$\tau_f = \frac{\delta}{\tau^2} \quad [9]$$

This results in a range of D_e from 2.8×10^{-12} to 3.1×10^{-12} m^2/s which is consistent with values reported for the Queenston Formation by Xiang et al. (2013) (Table 1). By propagating the error from the averaged ϕ_I values, and from multiple D_p values determined from C/C_0 data, uncertainty bounds were calculated for D_e to reflect heterogeneity within a single sample. When expressed as the relative standard deviation, these are on the order of 7.7–8.2% (presented as 1 σ in Table 3). The variation in D_e between samples is similar (9.7%) indicating that adjacent samples have indistinguishable diffusion properties.

3.3. Partial gas saturation

The radiographic measurements of gas saturation ($S_{g\text{-}I}$) represent the fraction of gas volume in the pore space relative to the total iodide-accessible pore volume (Equation (6)). This paper is focused on iodide diffusion, so we use this approach consistently throughout.

As expected, gas saturation values are much lower than those predicted by Equation (5) which indicates values of approximately 28% for P_1 = 68 atm. The profiles for gas saturation display cyclic variations that correlate with those observed in the profiles of ϕ_I (Fig. 3), with low and high points in the cycles reflecting the presence or absence, respectively, of secondary dolomite lenses (Fig. 4). The profiles are broadly U-shaped, with values at the influx and outflux boundaries ranging from 5 to 13%, and values midway along the length ranging from 2 to 5% (Fig. 3). This observation is consistent with the expectation that gas bubbles will nucleate and grow faster near the boundaries because porewater can be expelled more rapidly due to a higher pressure gradient. The decreasing degree of gas saturation inward from the boundaries is also expected because, as the volume of gas increases near the boundaries, the relative permeability for the aqueous phase decreases (Van Genuchten, 1980), slowing the expulsion of porewater from the interior. This leads to a corresponding increase in the time available for N_2 loss by diffusion, and the rate of diffusive loss of N_2 will increase with time because the diffusion coefficient for N_2 will increase as the gas phase grows (Reardon and Moddle, 1985).

The foregoing discussion considers processes operative within a porous media with uniform porosity and pore-size distribution, but porosity in the Queenston Formation shale is not uniformly distributed (Fig. 3) and, in general, a uniform pore-size distribution is unlikely. In this case, during the initial stages of depressurization and gas exsolution, a random distribution of gas nucleation sites might be expected throughout the pore spaces (Du and Yortsos, 1999), but for nuclei to grow into bubbles, porewater must be forced out of the rock sample by advection. Consequently, gas bubbles will grow preferentially in connected regions of the rock with relatively high permeability, and when these preferential pathways are connected by a continuous gas phase, a critical gas saturation will be reached, allowing flow of the gas phase (Firoozabadi et al., 1992). It is possible that critical gas saturation was reached near the boundaries of the samples, but almost certainly not in the interior regions of the samples.

The gas-ingrowth mechanism used for these experiments is similar to what might occur at a larger scale in a natural organic-rich shale when hydrocarbon gases build up and exceed solubility, causing partial gas saturation. It is different from the dewatering mechanism used by (Savoye et al., 2010, 2012, 2014, 2017), which may better reflect evaporative and drainage processes in wall rocks adjacent to underground excavations. Dewatering is similar to the gas-ingrowth mechanism in that it will begin with water loss in the largest pores, however with gas ingrowth, once critical gas saturation is reached, growth of the gas phase will diminish or cease (Du and Yortsos, 1999). If dewatering is accomplished by outflow of water, then the limit to dewatering should be reached at the percolation threshold, but if the water is removed by evaporation, or if a chemical potential gradient is employed, as with the osmotic technique used by Savoye et al. (2010, 2012, 2014, 2017), then water loss can continue via vapor-phase transfer and result in dewatering beyond the percolation threshold. Consequently, dewatering methods can generate a higher degree of gas saturation than gas exsolution and ingrowth.

3.4. Diffusion in partially saturated shale

Profiles of relative tracer concentrations (C/C_0) collected at different times in the partially saturated samples are shown in Fig. 5c and d. The consistent baseline for the profiles (baseline = 1) demonstrates that the gas-saturation profiles are stable through time. Ingrowth of 4% gas in sample DGR3-472-A results in a decrease of D_e by 22.3% from 3.1×10^{-12} to 2.5×10^{-12} m^2/s and 6.7% gas saturation in sample DGR3-472-B causes D_e to decrease by 20.3% from 2.8×10^{-12} to 2.3×10^{-12} m^2/s (Table 3). These data demonstrate that diffusive transport in these rocks is dominated by a small fraction of the pore space such that generation of a small amount of gas has a significant effect on diffusivity. The decrease in D_e is partially accounted for by the decrease in ϕ_I, but the dominant factor is a decrease in τ_f (decreased δ and/or increased τ).

Archie's 2nd law has commonly been used to describe diffusion and electrical conduction in variably saturated porous media (Archie, 1942; Hamamoto et al., 2009; Hamamoto et al., 2010; Marshall, 1959; Mualem and Friedman, 1991; Savoye et al., 2010, 2012, 2014).

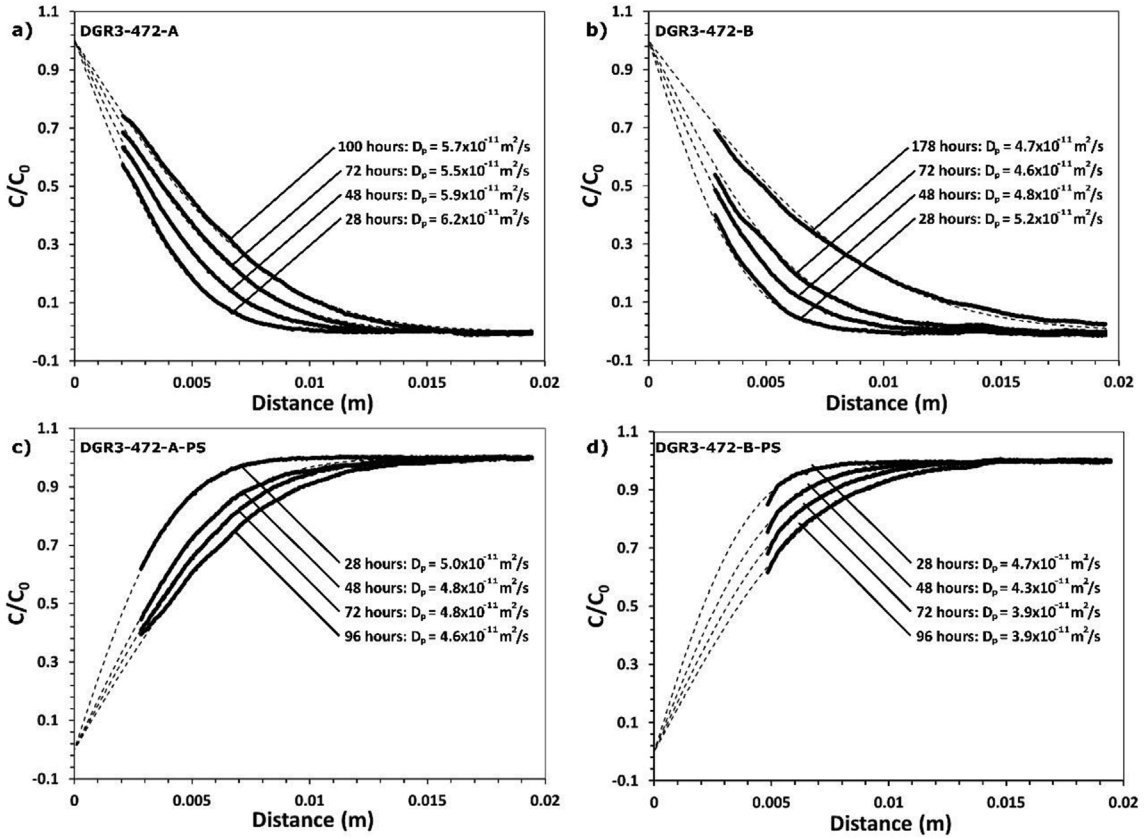

Fig. 5. One-dimensional, profiles of relative iodide concentration (C/C_0) collected at different times: a) in-diffusion experiment with 0% gas saturation (sample DGR-3-472.56-A), b) in-diffusion experiment with 0% gas saturation (sample DGR-3-472.56-B) c) out-diffusion experiment with 4.0% gas saturation (sample DGR-3-472.56-A), d) out-diffusion experiment with 6.7% gas saturation (sample DGR-3-472.56-B). The combined geometry of the samples and the cone-shaped X-ray beam causes some minor blurring of the signal near the boundaries, resulting in loss of data over a small distance. However, the fitting procedure relies on the whole data profile and the imposed boundary condition, so the influence of this data gap near the boundary on the D_p determination should be negligible.

According to Hamamoto et al. (2010), Archie's 2nd law can be described by Equations (10) and (11):

$$\frac{D_e}{D_0} = \phi_w^m \left[\frac{\phi}{\phi_w}\right]^n \quad [10]$$

$$\frac{D_e}{D_e^*} = \left[\frac{\phi}{\phi_w}\right]^n \quad [11]$$

where ϕ is the water-filled porosity under partially saturated conditions, D_e is the effective diffusion coefficient for iodide at a given saturation; D_e^* is the effective diffusion coefficient in the fully saturated sample, m is the cementation exponent and n is the saturation exponent. Archie's laws have been known to underestimate diffusivity and it has been suggested by many authors (Balberg, 1986; Hamamoto et al., 2010; Martys, 1999; Moldrup et al., 2007; Savoye et al., 2010) that there is a critical water saturation at which the water phase is no longer connected and transport through the porewater is no longer possible at a representative scale. Hamamoto et al. (2010) proposed a modified form of Archie's 2nd law to include a percolation threshold:

$$\frac{D_e}{D_0} = \left(\frac{\phi - \phi_{th}}{\phi_w - \phi_{th}}\right)^n * (\phi_w - \phi_{th}^*)^m \quad [12]$$

$$\frac{D_e}{D_e^*} = \left(\frac{\phi - \phi_{th}}{\phi_w - \phi_{th}}\right)^n \quad [13]$$

Where ϕ_{th}^* represents the fraction of the fluid phase that, under saturated conditions, does not participate in the solute-transport process, and ϕ_{th} represents the percolation threshold. In clay-rich rocks where diffusion is expected to be the dominant transport process, the assumption by Savoye et al. (2014) and Van Loon and Mibus (2015) that ϕ_{th}^* is equal to the fraction of the porewater that is inaccessible to anions is logical and seems reasonable. Furthermore, Hamamoto et al. (2010) and Savoye et al. (2014) suggested it can be assumed that ϕ_{th} is equal to ϕ_{th}^*.

Archie's laws are empirical relationships and there has been significant work directed at understanding the cementation exponent (m) in a variety of materials (Balberg, 1986; Boving and Grathwohl, 2001; Hunt, 2004; Revil and Cathles, 1999; Sen et al., 1981; Thompson et al., 1987; Van Loon and Mibus, 2015). In previous research on clay-rich rocks, m has been estimated to range from 2 to 3 (Descostes et al., 2008; Jacquier et al., 2013; Revil and Cathles, 1999; Savoye et al., 2010; Van Loon et al., 2003b; Van Loon and Mibus, 2015). Using Equation (12) and parameters presented in Table 3, we obtain values for m that fall in the same range (2.19 and 2.30 for DGR3-472-A and DGR3-472-B respectively; Table 4). There is a small number of published studies aimed toward understanding the values of the saturation exponent (n) for various materials. In soils and sands, values for both m and n roughly equal to 2 have been found to provide a good fit to many data sets (Archie, 1942; CRWMS M&O, 2000; Revil and Jougnot, 2008; Hamamoto et al., 2010; Thompson et al., 1987; Salem and Chilingarian, 1999). We are aware of only two studies (Savoye et al., 2010, 2014) that note values for n in clay rich rocks; they used a value of $n = 2$ but acknowledged that it was associated with significant uncertainty.

It is desirable to have a generalized empirical relationship such as Archie's 2nd law that could allow estimation of diffusion coefficients as a function of saturation. Based on Equation (13), this would require confidence in the determination of values for n and ϕ_{th}. As noted above,

Table 4
List of parameters used to estimate the range of values for n and ϕ_{th} with Equation (13).

	Estimate Values for n		Estimate Values for ϕ_{th}	
	DGR-3472.56-A	DGR-3472.56-B	DGR-3472.56-A	DGR-3472.56-B
Saturation exponent (n)	5.7	2.8	2	2
Percolation threshold (ϕ_{th})	0.048	0.043	0.082	0.059
Cementation exponent (m)	2.19	2.30	2.19	2.30
Inactive Fluid phase (ϕ_{th}*)	0.048	0.043	0.048	0.043
Water-accessible porosity (ϕ_w)	0.102	0.102	0.102	0.102

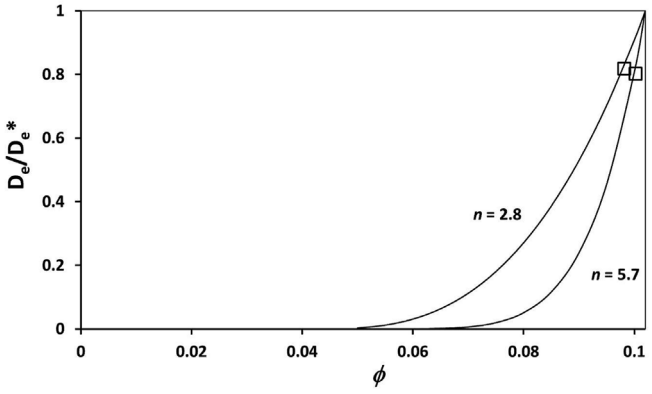

Fig. 6. Illustration based on Equation (13) to show variation in the iodide effective diffusion coefficient as a function of the water-filled porosity. Parameters are from Table 4. The square symbols represent measurements conducted in this study.

in clay-rich rocks where diffusion is the dominant transport process, it should be reasonable to assume that ϕ_{th}* is equal to the anion inaccessible porosity, and this parameter can be measured for I^- using the X-ray radiography technique described herein and by Cavé et al. (2009). However, desaturation and anion diffusion are very different processes, so we are less confident in the assumption that $\phi_{th} = \phi_{th}$* as suggested by Hamamoto et al. (2010) and Savoye et al. (2014). However, considering capillarity constraints on desaturation and anion-size constraints on diffusion, we expect that ϕ_{th}* should represent the lower bound for ϕ_{th}; or ϕ_{th}* $\leq \phi_{th}$. With little known about the value of n in clay-rich rocks, it is difficult to constrain, but since $n = 2$ has been used in previous studies (Savoye et al., 2010, 2014), we used that value in Equation (13) to calculate ϕ_{th}. Alternatively, we used the assumptions noted above that the anion-inaccessible porosity is equal to ϕ_{th}*, which in turn is equal to ϕ_{th}, to calculate n with Equation (13) (ϕ_{th}* = ϕ_w - $f_a \cdot \phi_w$). With this approach, we obtain values for n that range from 2.8 to 5.7, and values for ϕ_{th} that range from 0.059 to 0.082 (Table 4). The derived values for ϕ_{th} conform with our expectation that ϕ_{th}* $\leq \phi_{th}$, but in diffusion-dominated systems where ϕ_{th} is not known, but ϕ_{th}*can be determined from f_a, the best approach to understand the n exponent in Archie's 2nd law should be to assume $\phi_{th} = \phi_{th}$* and then calculate values for n with Equation (13). This method was used to generate the curves on Fig. 6 where it is obvious that when the degree of water saturation is high, diffusion coefficients obtained from Equation (13) are not highly sensitive to variations in n. This paper is primarily intended to present a new method for diffusion measurements with partially-saturated systems and it is clear that additional data are required to further refine Archie's 2nd law for clay-rich rocks.

4. Conclusions

This study successfully demonstrated a method to generate partial gas saturation in low-permeability shale with hypersaline porewater. The data indicate that small-scale heterogeneity in the porosity leads to similar variations in partial gas saturation. X-ray radiography was used to measure the change in $S_{g\text{-}I}$ in the iodide-accessible pore fraction in low permeability shale. Results are consistent with the expectation that an increase in partial gas saturation causes a decrease in D_e for aqueous solutes. The results indicate that τ_f is sensitive to partial saturation. When evaluating results in terms of Archie's 2nd law, the data indicate values for the n exponent ranging from 2.8 to 5.7, but more data are required over a greater range of gas saturations in order to better understand the value of this empirical approach. The high salinity of the natural porewater precludes the use of dewatering techniques, and the gas-ingrowth method presented in this paper is limited by the low permeability of the rocks such that N_2 losses by diffusion are significant before bubble growth can expel pore fluid. The gas ingrowth method is therefore prone to higher degrees of gas saturation at the ends of the sample. Future work will focus on samples with shorter length dimensions in an attempt to achieve higher, and more uniform gas distributions.

Acknowledgements

This work was supported by funding from the Nuclear Waste Management Organization (NWMO) and the Canadian Natural Science and Engineering Research Council (NSERC) (grant no. CRD 477852-14).

References

Agbogun, H.M.D., Al, T.A., Hussein, E.M.A., 2013a. Three dimensional imaging of porosity and tracer concentration distributions in a dolostone sample during diffusion experiments using X-ray micro-CT. J. Contam. Hydrol. 145, 44–53.
Agbogun, H.M.D., Hussein, E.M.A., Al, T.A., 2013b. Assessment of x-ray micro-CT measurements of porosity and solute concentration distributions during diffusion in porous geologic media. J. Porous Media 16, 683–694.
Al, T.A., Clark, I.D., Kennell, L., Jensen, M., Raven, K.G., 2015. Geochemical evolution and residence time of porewater in low-permeability rocks of the Michigan Basin, Southwest Ontario. Chem. Geol. 404, 1–17.
Appelo, C.A.J., Van Loon, L.R., Wersin, P., 2010. Multicomponent diffusion of a suite of tracers (HTO, Cl, Br, I, Na, Sr, Cs) in a single sample of Opalinus Clay. Geochem. Cosmochim. Acta 74, 1201–1219.
Archie, G.E., 1942. The electrical resistivity log as an aid in determining some reservoir characteristics. Trans. AIME 146, 54–62.
Badv, K., Faridfard, M.R., 2005. Laboratory determination of water retention and diffusion coefficient in unsaturated sand. Water, Air, Soil Pollut. 161, 25–38.
Balberg, I., 1986. Excluded-volume explanation of Archie's law. Phys. Rev. B 33, 3618.
Bazer-Bachi, F., Tevissen, E., Descostes, M., Grenut, B., Meier, P., Simonnot, M.-O., Sardin, M., 2006. Characterization of iodide retention on Callovo-Oxfordian argillites and its influence on iodide migration. Phys. Chem. Earth, Parts A/B/C 31, 517–522.
Beauheim, R.L., Roberts, R.M., Avis, J.D., 2014. Hydraulic testing of low-permeability silurian and ordovician strata, Michigan basin, southwestern Ontario. J. Hydrol. 509, 163–178.
Bensenouci, F., Michelot, J.L., Matray, J.M., Savoye, S., Lavielle, B., Thomas, B., Dick, P., 2011. A profile of helium-4 concentration in pore-water for assessing the transport phenomena through an argillaceous formation (Tournemire, France). Phys. Chem. Earth, Parts A/B/C 36, 1521–1530.
Benson, S.M., Cole, D.R., 2008. CO 2 sequestration in deep sedimentary formations. Elements 4, 325–331.
Boving, T.B., Grathwohl, P., 2001. Tracer diffusion coefficients in sedimentary rocks: correlation to porosity and hydraulic conductivity. J. Contam. Hydrol. 53, 85–100.
Cavé, L., Al, T., Xiang, Y., Vilks, P., 2009. A technique for estimating one-dimensional diffusion coefficients in low-permeability sedimentary rock using X-ray radiography: comparison with through-diffusion measurements. J. Contam. Hydrol. 103, 1–12.
CEAA, 2015. Joint Review Panel Environmental Assessment Report: Deep Geologic Repository for Low to Intermediate Level Radioactive Waste Project. CEAA Reference No. 17520. Ottawa, Canada. Report available online through. . https://www.ceaa-acee.gc.ca.
Clark, I.D., Al, T., Jensen, M., Kennell, L., Mazurek, M., Mohapatra, R., Raven, K.G., 2013. Paleozoic-aged brine and authigenic helium preserved in an Ordovician shale aquiclude. Geology 41, 951–954.
Conca, J.L., Wright, J., 1992. Diffusion and flow in gravel, soil, and whole rock. Hydrogeol. J. 1, 5–24.
Cormenzana, J.L., García-Gutiérrez, M., Missana, T., Junghanns, Á., 2003. Simultaneous estimation of effective and apparent diffusion coefficients in compacted bentonite. J. Contam. Hydrol. 61, 63–72.

Crank, J., 1979. The Mathematics of Diffusion. Oxford university press.
CRWMS M&O, 2000. Total System Performance Assessment for the Site Recommendation, TDR-WIS-PA-000001 REV 00. United States of America, Las Vegas, Nevada.
Desaulniers, D.E., Cherry, J.A., Fritz, P., 1981. Origin, age and movement of pore water in argillaceous Quaternary deposits at four sites in southwestern Ontario. J. Hydrol. 50, 231–257.
Descostes, M., Blin, V., Bazer-Bachi, F., Meier, P., Grenut, B., Radwan, J., Schlegel, M.L., Buschaert, S., Coelho, D., Tevissen, E., 2008. Diffusion of anionic species in Callovo-Oxfordian argillites and Oxfordian limestones (Meuse/Haute–Marne, France). Appl. Geochem. 23, 655–677.
Du, C., Yortsos, Y.C., 1999. A numerical study of the critical gas saturation in a porous medium. Transp. Porous Media 35, 205–225.
Firoozabadi, A., Ottesen, B., Mikklesen, M., others, 1992. Measurements of super-saturation and critical gas saturation (includes associated papers 27920 and 28669). SPE Form. Eval. 7, 337–344.
García-Gutiérrez, M., Cormenzana, J.L., Missana, T., Mingarro, M., Molinero, J., 2006. Overview of laboratory methods employed for obtaining diffusion coefficients in FEBEX compacted bentonite. J. Iber. Geol. 32, 37.
Gimmi, T., Waber, H.N., Gautschi, A., Rübel, A., 2007. Stable water isotopes in pore water of Jurassic argillaceous rocks as tracers for solute transport over large spatial and temporal scales. Water Resour. Res. 43.
Hamamoto, S., Perera, M.S.A., Resurreccion, A., Kawamoto, K., Hasegawa, S., Komatsu, T., Moldrup, P., 2009. The solute diffusion coefficient in variably compacted, un-saturated volcanic ash soils. Vadose Zone J. 8, 942–952.
Hamamoto, S., Moldrup, P., Kawamoto, K., Komatsu, T., 2010. Excluded-volume ex-pansion of Archie's law for gas and solute diffusivities and electrical and thermal conductivities in variably saturated porous media. Water Resour. Res. 46.
Hendry, M.J., Harrington, G.A., 2014. Comparing vertical profiles of natural tracers in the Williston Basin to estimate the onset of deep aquifer activation. Water Resour. Res. 50, 6496–6506.
Hendry, M.J., Kelln, C.J., Wassenaar, L.I., Shaw, J., 2004. Characterizing the hydro-geology of a complex clay-rich aquitard system using detailed vertical profiles of the stable isotopes of water. J. Hydrol. 293, 47–56.
Hendry, M.J., Barbour, S.L., Novakowski, K., Wassenaar, L.I., 2013. Paleohydrogeology of the Cretaceous sediments of the Williston Basin using stable isotopes of water. Water Resour. Res. 49, 4580–4592.
Hunt, A.G., 2004. Continuum percolation theory and Archie's law. Geophys. Res. Lett. 31.
Intera, 2011. Descriptive Geosphere Site Model, Revision 0. DGR-tr-2011-24. Intera Engineering Ltd. Report prepared for the Nuclear Waste Management Organization NWMO. Report available online through. . http://www.nwmo.ca.
Jackson, R., 2009. Organic Geochemistry and Clay Mineralogy of DGR-3 and DGR-4 Core, Revision 0. TR-08-29. Report prepared for Intera Engineering Ltd., November, 2009. Report available online through. . http://www.nwmo.ca.
Jacops, E., Volckaert, G., Maes, N., Weetjens, E., Govaerts, J., 2013. Determination of gas diffusion coefficients in saturated porous media: He and CH 4 diffusion in Boom Clay. Appl. Clay Sci. 83, 217–223.
Jacquier, P., Hainos, D., Robinet, J.C., Herbette, M., Grenut, B., Bouchet, A., Ferry, C., 2013. The influence of mineral variability of Callovo-Oxfordian clay rocks on radionuclide transfer properties. Appl. Clay Sci. 83, 129–136.
Javadpour, F., Fisher, D., Unsworth, M., others, 2007. Nanoscale gas flow in shale gas sediments. J. Can. Pet. Technol. 46.
Koroleva, M., de Haller, A., Mader, U., Waber, H.N., Mazurek, M., 2009. Borehole DGR-2: Pore-water Investigations, Revision 0. TR-08-06. Report prepared for Intera Engineering Ltd. (now Geofirma Engineering Ltd.), August, 2009. Report available online through. . http://www.nwmo.ca.
Leung, D.Y.C., Caramanna, G., Maroto-Valer, M.M., 2014. An overview of current status of carbon dioxide capture and storage technologies. Renew. Sustain. Energy Rev. 39, 426–443.
Lindeberg, E., Bergmo, P., 2003. The long-term fate of CO2 injected into an aquifer. Greenh. gas Control Technol. 1, 489–494.
Loomer, D.B., Scott, L., Al, T.A., Mayer, K.U., Bea, S., 2013. Diffusion–reaction studies in low permeability shale using X-ray radiography with cesium. Appl. geochemistry 39, 49–58.
Mao, S., Duan, Z., 2006. A thermodynamic model for calculating nitrogen solubility, gas phase composition and density of the N2–H2O–NaCl system. Fluid Phase Equil. 248, 103–114.
Marshall, T.J., 1959. The diffusion of gases through porous media. J. Soil Sci. 10, 79–82.
Martys, N.S., 1999. Diffusion in partially-saturated porous materials. Mater. Struct 32, 555–562.
Matray, J.M., Savoye, S., Cabrera, J., 2007. Desaturation and structure relationships around drifts excavated in the well-compacted Tournemire's argillite (Aveyron, France). Eng. Geol. 90, 1–16.
Mazurek, M., Alt-Epping, P., Bath, A., Gimmi, T., Waber, H.N., Buschaert, S., De Cannière, P., De Craen, M., Gautschi, A., Savoye, S., others, 2011. Natural tracer profiles across argillaceous formations. Appl. Geochem. 26, 1035–1064.
Mazurek, M., Oyama, T., Wersin, P., Alt-Epping, P., 2015. Pore-water squeezing from indurated shales. Chem. Geol. 400, 106–121.
Mehta, B.K., Shiozawa, S., Nakano, M., 1995. Measurement of molecular diffusion of salt in unsaturated soils. Soil Sci. 159, 115–121.
Moldrup, P., Olesen, T., Blendstrup, H., Komatsu, T., de Jonge, L.W., Rolston, D.E., 2007. Predictive-descriptive models for gas and solute diffusion coefficients in variably saturated porous media coupled to pore-size distribution: IV. Solute diffusivity and the liquid phase impedance factor. Soil Sci. 172, 741–750.
Mualem, Y., Friedman, S.P., 1991. Theoretical prediction of electrical conductivity in saturated and unsaturated soil. Water Resour. Res. 27, 2771–2777.
Nagra, 2008. Effects of Post-disposal Gas Generation in a Repository for Low- and Intermediate-level Waste Sited in the Opalinus Clay of Northern Switzerland. Nagra Technical Report NTB 08-07. Wettingen, Switzerland. Report available online through. . https://www.nagra.ch.
Olesen, T., Moldrup, P., Yamaguchi, T., Nissen, H.H., Rolston, D.E., 2000. Modified half-cell method for measuring the solute diffusion coefficient in undisturbed, unsaturated soil. Soil Sci. 165, 835–840.
Patriarche, D., Ledoux, E., Michelot, J.-L., Simon-Coinçon, R., Savoye, S., 2004a. Diffusion as the main process for mass transport in very low water content argillites: 2. Fluid flow and mass transport modeling. Water Resour. Res. 40.
Patriarche, D., Michelot, J.-L., Ledoux, E., Savoye, S., 2004b. Diffusion as the main pro-cess for mass transport in very low water content argillites: 1. Chloride as a natural tracer for mass transport—diffusion coefficient and concentration measurements in interstitial water. Water Resour. Res. 40.
Porter, L.K., Kemper, W.D., Jackson, R.D., Stewart, B.A., 1960. Chloride diffusion in soils as influenced by moisture content. Soil Sci. Soc. Am. J. 24, 460–463.
Reardon, E.J., Moddle, P.M., 1985. Gas diffusion coefficient measurements on uranium mill tailings: implications to cover layer design. Uranium 2, 111–131.
Rebour, V., Billiotte, J., Deveughele, M., Jambon, A., Le Guen, C., 1997. Molecular dif-fusion in water-saturated rocks: a new experimental method. J. Contam. Hydrol. 28, 71–93.
Remenda, V.H., Cherry, J.A., Edwards, T.W.D., 1994. Isotopic composition of old ground water from Lake Agassiz: implications for late Pleistocene climate. Science 5193, 266 1975.
Revil, A., Cathles, L.M., 1999. Permeability of shaly sands. Water Resour. Res. 35, 651–662.
Revil, A., Jougnot, D., 2008. Diffusion of ions in unsaturated porous materials. J. Colloid Interface Sci. 319, 226–235.
Rowell, D.L., Martin, M.W., Nye, P.H., 1967. The measurement and mechanism of ion diffusion in soils III. The effect of moisture content and soil-solution concentration on the self-diffusion of ions in soils. Eur. J. Soil Sci. 18, 204–221.
Russell, D.J., Gale, J.E., 1982. Radioactive waste disposal in the sedimentary rocks of southern Ontario. Geosci. Can. 9.
Salem, H.S., Chilingarian, G.V., 1999. The cementation factor of Archie's equation for shaly sandstone reservoirs. J. Petrol. Sci. Eng. 23, 83–93.
Savoye, S., Page, J., Puente, C., Imbert, C., Coelho, D., 2010. New experimental approach for studying diffusion through an intact and unsaturated medium: a case study with Callovo-Oxfordian argillite. Environ. Sci. Technol. 44, 3698–3704.
Savoye, S., Goutelard, F., Beaucaire, C., Charles, Y., Fayette, A., Herbette, M., Larabi, Y., Coelho, D., 2011. Effect of temperature on the containment properties of argillaceous rocks: the case study of Callovo–Oxfordian claystones. J. Contam. Hydrol. 125, 102–112.
Savoye, S., Beaucaire, C., Fayette, A., Herbette, M., Coelho, D., 2012. Mobility of cesium through the callovo-oxfordian claystones under partially saturated conditions. Environ. Sci. Technol. 46, 2633–2641.
Savoye, S., Lefevre, S., Fayette, A., Robinet, J.-C., 2017. Effect of water saturation on the diffusion/adsorption of 22Na and cesium onto the Callovo-Oxfordian claystones. Geofluids 2017, 1683979.
Savoye, S., Imbert, C., Fayette, A., Coelho, D., 2014. Experimental study on diffusion of tritiated water and anions under variable water-saturation and clay mineral content: comparison with the Callovo-Oxfordian claystones. Geol. Soc. London, Spec. Publ. 400, 579–588.
Sen, P.N., Scala, C., Cohen, M.H., 1981. A self-similar model for sedimentary rocks with application to the dielectric constant of fused glass beads. Geophysics 46, 781–795.
Shackelford, C.D., 1991. Laboratory diffusion testing for waste disposal—a review. J. Contam. Hydrol. 7, 177–217.
Thompson, A.H., Katz, A.J., Krohn, C.E., 1987. The microgeometry and transport prop-erties of sedimentary rock. Adv. Phys. 36, 625–694.
Tidwell, V.C., Meigs, L.C., Christian-Frear, T., Boney, C.M., 2000. Effects of spatially heterogeneous porosity on matrix diffusion as investigated by X-ray absorption imaging. J. Contam. Hydrol. 42, 285–302.
Van der Kamp, G., Van Stempvoort, D.R., Wassenaar, L.I., 1996. Using intact cores to determine isotopic composition, chemistry and effective porosities for groundwater in aquitards. Water Resour. Res. 32, 1815–1822.
Van Genuchten, M.T., 1980. A closed-form equation for predicting the hydraulic con-ductivity of unsaturated soils. Soil Sci. Soc. Am. J. 44, 892–898.
Van Loon, L.R., Mibus, J., 2015. A modified version of Archie's law to estimate effective diffusion coefficients of radionuclides in argillaceous rocks and its application in safety analysis studies. Appl. Geochem. 59, 85–94.
Van Loon, L.R., Soler, J.M., Bradbury, M.H., 2003a. Diffusion of HTO, 36 Cl- and 125 I- in opalinus clay samples from mont terri: effect of confining pressure. J. Contam. Hydrol. 61, 73–83.
Van Loon, L.R., Soler, J.M., Jakob, A., Bradbury, M.H., 2003b. Effect of confining pressure on the diffusion of HTO, 36 Cl- and 125 I- in a layered argillaceous rock (Opalinus Clay): diffusion perpendicular to the fabric. Appl. Geochem. 18, 1653–1662.
Van Loon, L.R., Soler, J.M., Müller, W., Bradbury, M.H., 2004. Anisotropic diffusion in layered argillaceous rocks: a case study with Opalinus Clay. Environ. Sci. Technol. 38, 5721–5728.
Van Loon, L.R., Glaus, M.A., Müller, W., 2007. Anion exclusion effects in compacted bentonites: towards a better understanding of anion diffusion. Appl. Geochem. 22, 2536–2552.
Waber, H.N., Smellie, J.A.T., 2008. Characterisation of pore water in crystalline rocks. Appl. Geochem. 23, 1834–1861.
Wise, D.L., Houghton, G., 1966. The diffusion coefficients of ten slightly soluble gases in water at 10–60 C. Chem. Eng. Sci. 21, 999–1010.
Xiang, Y., Al, T., Scott, L., Loomer, D., 2013. Diffusive anisotropy in low-permeability Ordovician sedimentary rocks from the Michigan Basin in southwest Ontario. J. Contam. Hydrol. 155, 31–45.
Xiang, Y., Al, T., Mazurek, M., 2016. Effect of confining pressure on diffusion coefficients in clay-rich, low-permeability sedimentary rocks. J. Contam. Hydrol. 195, 1–10.